

**The Role of a Massive Central Singularity in Galactic Mergers on
the Survival of the Core Fundamental Plane.**

Kelly Holley-Bockelmann and Douglas O. Richstone

Astronomy Department, University of Michigan

Received _____; accepted _____

arXiv:astro-ph/9908258v1 24 Aug 1999

ABSTRACT

In order for the core Fundamental Plane (cFP) to endure, small ellipticals must not survive mergers with giant ellipticals, despite the fact the small secondary galaxy can be as much as a million times more dense than the primary. However, our previous set of experiments has shown that, for purely stellar galaxies, the secondary does in fact survive mergers with primaries up to 100 times more massive. In this paper, we demonstrate the effect that a massive central black hole has on mergers of cFP galaxies. Our results indicate that the addition of a massive central singularity inside the primary galaxy provides strong enough tidal forces to destroy dense cFP companions when the secondary’s orbital decay is sufficiently elongated. The destruction of the secondary acts to preserve the original low central density profile of the primary in the giant merger remnant, which allows the remnant to remain on the cFP. On more circular orbits, though, the secondary is only disrupted near the end of the merger, and the degree to which the secondary particles disperse depends on the amount of orbital energy left in the merger. Hence, there are some mergers for which the cFP is not preserved in our experiments. We find that if the secondary is not dispersed, it forms a spinning stellar disk with a central density that forces the merger remnant off the cFP.

Subject headings: stellar dynamics - galaxies: kinematics and dynamics -galaxies: evolution - galaxies: clusters - galaxies: nuclei - galaxies: elliptical

1. Introduction

Although elliptical galaxies may evolve passively, there is considerable evidence that at least some ellipticals evolve by merging. For example, counterrotating cores can be explained by the recent accretion of a spinning galaxy, especially when accompanied by a secondary starburst (Kormendy, 1984; Franx & Illingworth, 1988; Carollo *et al*, 1997). Mergers are also thought to be responsible for the apparent bimodality of globular cluster populations (Kissler-Patig *et al*, 1998; Whitmore, 1997; Ashman & Zepf, 1992), and for structural changes like multiple nuclei, dust lanes, circumnuclear shells, and boxy isophotes (Malin & Carter, 1983; Schweizer, 1982; Seitzer & Schweizer, 1990; Forbes & Thomson, 1992).

To the extent that elliptical galaxies evolve by satellite accretion, it is difficult for a large, gas-poor elliptical galaxy to preserve a low density core, because the accretion of a small, high density satellite will steepen the inner density profile of the merger remnant (Faber *et al*, 1997), provided the secondary survives. This is the paradox of the core Fundamental Plane (cFP). The cFP demonstrates that elliptical galaxy centers maintain a tight relationship between projected central density and luminosity, a relationship foreshadowed independently by Lauer and Kormendy 15 years ago (Kormendy, 1985; Lauer, 1985). If, however, a secondary survives in a high density ratio merger (that is: if the central phase space distribution of the secondary and its debris has not dispersed compared to its original state), then the merger remnant will not lie on this plane. So, if even a fraction of large ellipticals accrete dense cFP secondaries, we would expect considerable scatter at the bright end of the cFP.

A massive black hole at the center of large galaxies may preserve the cFP by tidally disrupting dense secondaries in the accretion process. Observations are beginning to show that massive central black holes are a natural part of galaxy centers (Richstone *et al*,

1998), and as a consequence, their effects ought to be included in calculations of galaxy mergers. Current dynamical estimates of the best galactic black hole candidates have yielded masses on the order of $0.005M_{\text{bulge}}$ (Magorrian *et al*, 1998; Kormendy & Richstone, 1995). Such massive black holes dominate the galactic potential inside the cusp radius, $r_{\text{cusp}} \approx GM_{\bullet}/\sigma_{\text{bulge}}^2$, where M_{\bullet} is the black hole mass, and σ_{bulge} is the velocity dispersion of the bulge. This cusp radius can be on the order of a kiloparsec for the largest ellipticals, which is not a small fraction of the core radius and can, in some cases, be resolved.

Despite the importance of black holes to elliptical galaxy centers, simulating the effects of a massive black hole on the stellar distribution unfortunately presents a numerical challenge. Stellar velocities increase as $r^{-1/2}$ near the black hole, and the tiny timestep required to accurately track these stars is prohibitively expensive. In addition, the steep gradient in the potential near a black hole must be well resolved, and this typically requires a very large particle number (see however Sigurdsson *et al*, 1995). Nonetheless, there has been significant work done both on developing realistic galaxy models with central singularities (Merritt & Quinlan, 1998; Sigurdsson *et al*, 1995), and on simulating the effect that black hole binaries have on the host galaxy (Makino & Ebisuzaki, 1996; Governato *et al*, 1994). In addition, the analysis of an ensemble of individual stellar orbits within a black hole embedded galaxy may indicate the destabilizing influence of a black hole on a galaxy’s orbital structure (Merritt & Valluri, 1998).

In a previous paper, we showed that for purely stellar cFP galaxies, a secondary survives any merger in which it is more dense than the primary (Holley-Bockelmann & Richstone, 1999, hereafter paper 1). In this paper, we isolate the effect of a single massive black hole in these encounters by adding a black hole to the primary galaxy. As in paper 1, the primary is rigid, so the addition of a black hole can be modeled as an external force on the secondary. While the secondary is separated from the black hole (or if the encounter

is impulsive), there is no need to invoke a tiny timestep or an increased particle number in the secondary. This approach is an efficient way to determine whether massive central black holes can destroy a dense satellite during a merger. In this paper, we apply the method developed to problem of secondary destruction. We begin with a review of our approximation method in § 2. For details of the technique, in particular for tests of both the rigid primary approximation and our particle-field code, please refer to paper 1. The tests of the black hole embedded method and results of our simulations can be found in § 3. Section 4 discusses the implications of the results on the persistence of the cFP and previews future work.

2. Methods

2.1. The Galaxy Models

We used the same technique as in paper 1 for choosing initial conditions, and for defining, modeling and populating galaxies on the cFP. See Table 1 for galaxy parameters and black hole masses. Our galaxies were initially composed of 5000 particles distributed over both the core and the envelope of our galaxies. For each mass ratio, a test merger was run, and the particle loss of the envelope was analyzed. To achieve better central resolution, we conducted the merger again, this time assigning 5000 particles to only the central regions of the secondary under the assumption that the galaxy envelope behaved in the same manner as in our test run. Table 2 presents the spatial resolution for our double and single component galaxy models. We followed only the particles that were bound to the secondary, but we preserved the phase space, energy, and angular momentum information of the unbound particles at the time they were stripped from the secondary. We will concentrate on the better resolved results for the 5000 particle single component galaxies, also referred to as inner η models.

2.2. The Force on the Secondary

Since the addition of a central black hole introduces a force that does not tend smoothly to zero at the center of the primary, we chose not to use a tidal approximation of the external force, as we did in paper 1. Instead, we advanced the particles in the inertial frame, where the force on a secondary particle is:

$$\vec{F}_{\text{tot}}(\vec{R}) = \vec{F}_2(\vec{r}) + \vec{F}_1(\vec{R})^* + \vec{F}_{\text{fric}}(\vec{R}) + \vec{F}_\bullet(\vec{R}), \quad (1)$$

where \vec{F}_2 is the self gravity of the secondary, \vec{F}_1^* is the force on a secondary particle due to the stars in the primary, \vec{F}_{fric} is the force due to dynamical friction, \vec{r} is the vector which points from the secondary center to a secondary particle, \vec{R} is the vector which points from the primary center to the secondary particle, and \vec{F}_\bullet is the force due to the black hole, expressed as:

$$\vec{F}_\bullet(\vec{R}) = -\frac{GM_\bullet m_p}{(\vec{R} + \epsilon)^3} \vec{R}, \quad (2)$$

where ϵ is a softening parameter which we chose to be close to the core radius of the secondary, and M_\bullet was chosen to be consistent with the Kormendy & Richstone relation (1995). Our softening parameter is much larger than the spatial resolution in our inner η models, but we chose this larger ϵ because it was consistent with the spatial resolution in the double η model galaxies here and in paper 1, and we wanted to be sure that we were isolating the effect of the black hole when we compared our results to our previous experiments. With this degree of softening, the experiments are designed to represent a lower limit to the damage done to dense secondaries.

2.3. The Dynamical Friction on a Secondary Particle

We apportioned the total dynamical friction force, F_{fric} , equally to each secondary particle (see appendix A). The frictional acceleration applied to each particle in the secondary galaxy, $d\vec{v}_f/dt$, is derived from the Chandrasekhar formula and is a function of a secondary’s position in the primary galaxy:

$$\frac{d\vec{v}_f(\vec{R})}{dt} = -f_{\text{drag}} 4\pi \ln\Lambda G^2 \rho_1 m_2(t) \left[\text{erf}(X) - \frac{2X}{\sqrt{\pi}} e^{-X^2} \right] \frac{\vec{v}_2}{v_2^3}, \quad (3)$$

where \vec{v}_2 is the velocity of the secondary, $X \equiv v_2/(\sqrt{2}\sigma)$, $\sigma = \sqrt{0.4GM_1/r_{1,\text{eff}}}$, Λ is the Coulomb logarithm which was set to M_1/M_2 , and f_{drag} is a drag coefficient, as explained in paper 1. We allowed the total mass of the secondary galaxy, $m_2(t)$ to vary as mass is lost in the merger.

Mass lost by the secondary will decrease the magnitude of the dynamical friction force, and will change the orbital decay trajectory such that the secondary experiences more pericenter passes. Analysis of the purely stellar simulations from paper 1 indicate that the secondary was stripped at each pericenter pass down to its tidal radius, $r_{\text{tide}}^3 \approx M_1/M_2 D^3$. We incorporated this knowledge into our set of black hole simulations. We initially set the mass of the secondary in a_{fric} equal to the total secondary mass, and when the secondary encountered a pericenter pass that was within the core radius of the primary, we reset the total mass to the mass enclosed by the tidal radius. ¹

¹We did not include secondary mass loss in the orbital decay calculations in paper 1. Therefore, we simulated the purely stellar 10:1 merger from paper 1 again with an orbital trajectory that included mass loss in the dynamical friction term as described above. Since the secondary remained intact, we can be certain that it was not the change in the orbital decay that destroys the secondary in our black hole experiments (figure 1).

This two part mass loss scenario was selected for reasons of computational speed, since a continuous mass loss term in the orbital decay would result in a larger number of orbits that are far from the damaging black hole potential. These large apocenter orbits take a long time to integrate, and most of the integration is spent following a secondary that is too far from the center of the primary to feel a significant external force. While this scheme underestimates the change in the dynamical friction force, resulting in fewer pericenter passes than in reality, it is useful as a limiting experiment: if the secondary breaks up after a few pericenter passes, it would certainly break up after more.

3. Results

As in paper 1, we explore a 2-dimensional grid of parameter space. In the first dimension, we vary the mass ratio, and in the second dimension, we vary the initial orbital angular momentum of the secondary. In this section, the results are organized in groups of differing angular momentum. Since our goal is to investigate the effect of a single massive black hole on the breakup or survival of dense secondaries in mergers with primaries, we first sought to duplicate the plunging encounters we explored in paper 1. In this way, we can isolate the damage generated by the black hole. For a summary of the different experiments conducted, see table 3.

3.1. Plunging Orbits

Anticipating that the most damaging effect would be due to tidal forces experienced as the secondary passes through the center of the primary, we launched a series of nearly parabolic, plunging orbits. In this basic set of experiments, we investigated two mass ratios: 100:1, 10:1. These mass ratios correspond to density ratios of approximately 1:830 and

1:105 at a radius of 0.1 pc, and the density ratio rapidly increases at smaller radii. We focus on the 10:1 simulation. Figure 2 shows the time evolution of the secondary in the force field of the primary. Here, we learn that most of the mass is stripped at pericenter, and comes off impulsively in a cloud which continues to expand as the secondary crosses the primary center again. However, it is apparent that the impulsive injection of energy into the secondary by the black hole is not enough to disrupt the secondary after the first pericenter pass. From the impulse approximation, the first order change in energy of the secondary due to the black hole,

$$\Delta E/E \approx (M_{\bullet}/M_2) (\sigma_2/v_{\text{orb}}) (R_{\text{core}}/P), \quad (4)$$

is of order 10^{-2} on the first pass. Instead, the secondary remained intact inside the tidal radius, $r_{\text{tide}}^3 \approx M_1/M_2 S^3$, for approximately 5 more pericenter passes, until enough energy was pumped into the secondary to unbind it. In figure 3, we illustrate the change in the secondary energy from beginning to end for this merger. The stripped mass is still bound to the primary and is spread out over a volume of space with a radius of approximately 250 parsecs from the black hole, or roughly the second apocenter distance. With the secondary disrupted over so large a volume, the merger remnant will remain on the cFP. Figure 4 illustrates the change in the secondary density profile for the 10:1 mass ratio. For the 100:1 mass ratio, the secondary density profile and snapshots of the secondary during the merger are presented in figures 5 and 6, respectively. To ensure that the secondary’s disruption was not an error caused by pericenter passes directly through the black hole, we also conducted a $\kappa = 0.05$, 100:1 experiment (figure 7), in which the first pericenter pass was approximately 400 parsecs from the black hole, on the order of the core radius of the primary. In all three experiments, the secondary was destroyed. This is a markedly different result from the purely stellar case where the secondary remained intact, and indicates the importance of

massive black holes as a source of impulsive energy during mergers.

3.2. Small Black Hole Mass

To confirm that the black hole is the direct cause of the secondary’s destruction, we launched a zero angular momentum 10:1 mass ratio encounter in which the primary was host to a black hole with about 0.005% the mass of the secondary, or nearly $9 \times 10^6 M_{\odot}$. In this case, the center region of the secondary was preserved (figure 8). We interpret this result as evidence that our method can detect a secondary’s disruption yet does not force disruption erroneously through the simple existence of a singularity. It is conceivable that the cFP can put a constraint on the mass of central black holes, independent of AGN light predictions; clearly, when the black hole mass is down by a factor of over 300 from the ridgeline, as it is in this experiment, the mass is not sufficient to destroy a secondary. Faber *et al*, 1997 presents a similar argument that the central black hole mass is constrained by the mass of the stellar core profile that forms around a binary black hole pair.

3.3. Non-radial Secondary Orbits

3.3.1. Secondary Destruction

To explore the effect that different orbits have on the preservation of the cFP, we launched secondaries in the 10:1 and 100:1 mass ratios on orbits with significant angular momentum. Our orbits are parameterized by $\kappa \equiv L/L_{\text{circ}}$. In the 10:1 mass ratio, we selected $\kappa = 0.2, 0.8$, and for the 100:1 case, we chose $\kappa = 0.5$. Figure 9 displays an xy plane projection of the first few orbits in each of these trajectories.

In each of these experiments, the secondary was stripped to the tidal radius at the

last pericenter of the the orbit. However, since the secondary is far from the black hole on all but the last few pericenter passes, this tidal radius is quite large for most of the decay trajectory. The secondary’s core is therefore intact through all but the last passes, since the density at the secondary core is clearly greater than the stellar component of the primary everywhere. In the final passes, the black hole can exert significant tidal forces on the secondary, and the secondary is actually tidally compressed in two dimensions, which increases its central density profile briefly in projection.

On any given orbit, the secondary will eventually reach a place in the merger where the force exerted by the black hole is enough to overpower the secondary self gravity and it is destroyed. Roughly speaking, this occurs the first time the galaxy passes through a region where:

$$\frac{M_{\bullet}}{P^3} > \frac{M_2}{r_2^3}, \quad (5)$$

where P is the distance of a pericenter pass, M_{\bullet} is the black hole mass, and r_2 is the core radius of the secondary. Strictly speaking, all of our non-radial mergers resulted in the destruction of the secondary. However, it is insufficient to equate secondary damage with success in protecting the cFP. While it is true that the core Fundamental Plane requires the disruption of dense secondaries in mergers, it is *not* true that the mere disruption of secondary necessarily results in a remnant that lies on the cFP. At disruption, the particles inherit the orbital energy of the secondary, and for the particles to be dispersed, the disruption must occur while there is still enough orbital energy to carry the debris out to a large apocenter so that the density of the debris is reduced to the density of the remnant. Otherwise, the remnant has too steep a central density profile to remain on the cFP. This can condition be stated as a function of the first post disruption apocenter:

$$\frac{M_1}{r_1^3} \approx \frac{M_2}{A^3}, \quad (6)$$

where r_1 is the core radius of the primary and A is the first post disruption apocenter. For the purposes of this paper, we define destruction to occur only when the debris is spread over a large enough apocenter to result in a significantly lower density profile. Likewise, we define the disruptions that occur only when the merger is effectively complete to be survivals.

Under this definition of destruction, the secondaries in the 10:1 $\kappa = 0.2$ and $\kappa = 0.8$ survived. See figures 10 and 11 for the change in the density profile of the secondary for the 10:1, $\kappa = 0.2$ and 10:1, $\kappa = 0.8$ experiments, respectively. The secondary in the 100:1, $\kappa = 0.5$ merger, however, was destroyed. Figure 12 shows the density profile for the 100:1, $\kappa = 0.5$ encounter. In fact, from our derived destruction criterion, we predict that for these galaxy parameters and our choice of dynamical friction, *all* orbits in the 100:1 mass ratio will result in destruction.

We caution that the distance of the first post disruption apocenter depends critically on the magnitude of the dynamical friction force at pericenter, which itself depends on the shape of the primary density profile and the mass of the secondary. For larger mass ratios (ie smaller secondary mass), since the dynamical friction is weaker, the orbit retains considerable orbital energy, and therefore experiences larger apocenters. Hence it is easier for the 100:1 case to disrupt than the 10:1 case. Similarly, a flat central primary density profile produces less dynamical friction at pericenter than a primary with a steep central density. Therefore, an $\eta = 3.0$ primary are more likely to disrupt a secondary than an $\eta = 1.0$ primary for a given mass ratio. With these conclusions, we numerically integrated several orbits with various mass ratios and primary density profiles and applied the disruption criteria in equation 5 (figure 13). From these results, we predict that if we

were to run our 10:1, $\kappa = 0.5$ experiment with an $\eta = 3.0$ primary, the secondary would be *destroyed*, due mostly to the flatness of the central primary density.

Although our results are not general, in that they appear to depend on the choice of the primary, we note the following important result: these experiments have produced a set of mergers that were not destroyed by the addition of a massive central black hole. Black holes, then, do not universally protect the cFP. Additionally, we discovered that the preservation of the cFP depends critically on the character of the orbit at the end of the merger.

3.3.2. Disk Formation

For non-radial mergers, the final part of the orbit produces interesting qualitative changes in the secondary as well. We define P_2 to be a pericenter pass that occurs before the secondary is disrupted. If P_2 is on the order of the core radius of the secondary, as was the case for the 10:1, $\kappa = 0.2$ and $\kappa = 0.8$ experiments, then the secondary is tidally torqued into a spinning disk with the radius of P_2 (orbital angular momentum is transferred into spinning up the secondary). A sense of the spin and a suggestion that the secondary is tidally torqued in the $\kappa = 0.8$ experiment may be seen in figure 14. Figure 15 shows the flattening induced, in part, by the spin in the $\kappa = 0.2$ encounter, and figure 16 illustrates the increase in the secondary spin for this experiment. Since the stellar disk begins to spin as it is still in the final orbits, it can be displaced from the primary center for a short time. For our $\kappa = 0.2$ merger, the spinning stellar disk was detectably off center for approximately 7×10^7 years. This is reminiscent of the off-center dust disk observed in NGC 4261 (Ferrarese *et. al.*, 1996). At the end of the simulation, we have a non self-gravitating central spinning stellar disk, which has some resemblance to the stellar disk in NGC 3115 (Kormendy *et. al.*, 1996). However, with an aspect ratio of 4:1, the disk we have formed is much thicker

than NGC 3115, which has an aspect ratio of 100:1. It is possible that with the addition of gas dynamics to our simulations, energy loss through gas dissipation could form a disk as thin as NGC 3115.

In the 10:1, $\kappa = 0.2$ and $\kappa = 0.8$ encounters, the high angular momentum particles were stripped preferentially from the forming disk, and by the time disk reaches the primary center, mostly plunging orbits were left. These plunging orbits become unbound to the secondary when they pass close to the black hole, so the secondary is dissolved within a few crossing times of reaching the center (although again, this denotes survival in our definition, because the debris is as tightly bound to the remnant as it was to the secondary.). Figure 17 shows the energy/angular momentum distribution for the $\kappa = 0.2$ experiment.

4. Discussion

We have investigated the effect a massive black hole at the center of an otherwise purely stellar primary has on mergers of high density ratio galaxies on the cFP.

We have concluded that the amount of damage that the black hole can inflict on the secondary during a merger is highly dependent on the orbital decay trajectory of the secondary. If the secondary's orbital decay is deeply plunging, the secondary encounters the black hole potential impulsively, and through repeated impulsive encounters, the black hole pumps enough energy into the secondary to unbind it.

If the secondary's encounter is non-radial, the secondary is far outside the radius of influence of the black hole for most of the merger, and it is stripped merely to the Roche radius. In our simulations, the damage done to the secondary center during this early stage is quite minimal. Only on the final few orbits does the galaxy sink close enough to the black hole to experience significant tidal stripping, which eventually unbinds the dense

secondary center. However, unless the disruption occurs while the merger has sufficient orbital energy, the debris orbits tightly around the center of the primary, and the remnant density is increased.

An important feature of the merger trajectory is the dependence on the density profile of the primary. In primaries with shallow density profiles and embedded black holes, the dynamical friction acting at the disruption is smaller than in primaries with steep density profiles, so the debris is more easily dispersed. For these galaxies, a much wider range of secondary masses will be destroyed (that is: disrupted such that $\rho_1 \approx \rho_2$).

It is tempting to identify this feature with the dichotomy between the central light profiles of bright and faint galaxies. Faber *et al.* 1997 note that galaxies brighter than about $M_v = -21$ have shallow, low density cores (their projected surface brightnesses $-d\log I/d\log r < 0.5$), while fainter ones are steeper. In our experiments, galaxies brighter than $M_v = -21.7$ destroy high mass ratio secondaries much more efficiently than fainter ones. Further investigation of this result seems worthwhile.

A proper understanding of the preservation of the cFP requires knowledge of the distribution of mass ratios and impact parameters of present day bulges. This can perhaps be computed reliably in virialized clusters (Tormen, 1997), where the galaxies encounter unbound targets. In this case, low-mass secondaries tend to merge on more circular orbits. The situation is likely to be quite different in a cold Hubble flow, where progenitors encounter each other only if they are on bound orbits, and where the orbits are likely to have little angular momentum (Aarseth & Fall, 1980). It is hard to believe, however, that progenitors of bulges encounter each other with *no* angular momentum, so it is not completely clear whether this work indicates the true resolution to the paradox of the cFP, or whether additional physics is needed in our experiments to explain the persistence of the cFP.

If *both* the galaxies in a cFP merger have central black holes, then a black hole binary may form in the center of the merger remnant, and 3 body scattering may heat the center and lower the remnant’s central density, allowing it to lie on the cFP. Apparently, there is some debate as to whether black hole binaries form from high mass ratio mergers (Governato, *et al.* , 1994). However, for equal mass mergers, Makino & Ebisuzaki (1996), and Quinlan & Hernquist (1997) found considerable black hole binary heating. As a consequence, the high central density from the more circular encounters in this paper may be disrupted upon the introduction of a black hole in the secondary, as long as the black holes form a binary pair. If so, this may be a powerful case that a black hole resides in the center of every galaxy. We will present the results of the effects of multiple black holes in cFP mergers in a future paper.

A second interesting feature of these results is the formation of rapidly spinning disks. When the secondary is not destroyed on a non-radial encounter, it can begin to spin during the final orbits as it is torqued by the black hole. Spinning stellar disks have been observed in many galaxies (such as NGC 3115, Capaccioli *et al.* , 1987), and have been invoked to explain apparent multiple nuclei in others (M31, Tremaine, 1995; NGC 4486b, Lauer *et al.* , 1996). Our purely stellar simulations form rather thick disks, with aspect ratios of approximately 4:1. However, the formation of fat stellar disks seems inevitable in these mergers. To form a disk as razor thin as NGC 3115 would most likely require a dissipative component. Nonetheless, non-radial galaxy mergers appear to be an efficient way to make a spinning stellar disk, as long as one of the galaxies is embedded with a massive central black hole.

Some support for this work was provided by the Space Telescope Science Institute, through general observer grant GO-06099.05-94A, and by NASA through a theory grant G-NAG5-2758. We thank the members of the NUKER collaboration for helpful

conversations. DR thanks the John Simon Guggenheim Foundation for a Fellowship.

REFERENCES

- Aarseth, S. J., & Fall, S. M., 1980, *ApJ*, 236, 43
- Ashman, K., & Zepf, S., 1992, *ApJ*, 384, 50
- Capaccioli, M., Held, E., Nieto, J.-L. 1987, *AJ*, 94, 1
- Carollo, C., Franx, M., Illingworth, G. D., Forbes, D. 1997, *ApJ*, 481, 710
- Faber, S., Kormendy, J., Byun, Youg-Ik, Dressler, A., Grillmair, C., Lauer, T., Richstone, D., Gebhardt, K., Tremaine, S. 1997, *AJ*, 114, 1771
- Ferrarese, L., Ford, H. C., Jaffe, W. 1996, *ApJ*, 470, 444
- Forbes, D. A., & Thomson, R. C. 1992, *MNRAS*, 254, 723
- Franx, M., & Illingworth, G. D. 1988, *ApJ*, 327, 55
- Governato, F., Colpi, M., Maraschi, L. 1994, *MNRAS*, 271, 317
- Holley-Bockelmann, K., & Richstone, D. 1999, *ApJ*, 517, 92
- Kissler-Patig, M., Forbes, D., Minniti, D. 1998, *MNRAS*, 298, 1123
- Kormendy, J. 1984, *ApJ*, 287, 577
- Kormendy, J. 1985, *ApJL*, 292, L9
- Kormendy, J. & Richstone D. 1995, *Ann Rev Astron and Astroph*, 33, 581
- Kormendy, J., Bender, R., Richstone, D., Ajhar, E. A., Dressler, A., Faber, S. M., Gebhardt, K., Grillmair, C., Lauer, T., Tremaine, S. 1996, *ApJ*, 459, L57
- Lauer, T. 1985, *ApJ*, 292, 104
- Lauer, T., Tremaine, S., Ajhar, E., Bender, R., Dressler, A., Faber, S., Gebhardt, K., Grillmair, C., Kormendy, J., Richstone, D. 1996, *ApJ*, 471, 79
- Makino, J., & Ebisuzaki, T. 1996, *ApJ*, 465, 527

- Malin, D. F., & Carter, D. 1983, ApJ, 274, 534
- Merritt, D., & Quinlan, G. 1998, ApJ, 498, 625
- Merritt, D., & Valluri, M. 1998, ApJ, 509, 933
- Quinlan, G., & Hernquist, L. 1997, New Astronomy, 2, 533
- Richstone D., Ajhar, E. A., Bender, R., Bower, G., Dressler, A., Faber, S., Filippenko, A. V., Gebhardt, K., Green, R., Ho, L. C., Kormendy, J., Lauer, T. R., Magorrian, J., Tremaine, S. 1998, Nature, 1998, 395, 14
- Schweizer, F. 1982, ApJ, 252, 455
- Seitzer, P., & Schweizer, F. 1990, PASP, 102, 615
- Sigurdsson, S., Hernquist, L., Quinlan, G. 1995, ApJ, 446, 75
- Tormen, G. 1997, MNRAS, 290, 729
- Tremaine, S. AJ, 1995, 110, 628
- Whitmore, B. 1997, IAUS, 186, 74

A. Appendix A

Under the impulse approximation, any single particle with mass m experiences a deflection, Θ , when traveling with a velocity \vec{v} past a single massive particle of mass M as follows:

$$\Theta = 1/v \int \frac{GM}{r^2} \frac{b}{r} \frac{dx}{v}, \quad (\text{A1})$$

where b is the impact parameter and dx is an infinitesimal distance in the velocity direction. In this simple case:

$$\Theta = \frac{1}{v^2} \frac{2GM}{b}. \quad (\text{A2})$$

The change in momentum in the direction of motion for this particle, Δp_{\parallel} , is:

$$\Delta p_{\parallel} = mv(\cos\Theta - 1), \quad (\text{A3})$$

which for small Θ can be expressed as:

$$\Delta p_{\parallel} = -\frac{2G^2 M^2 m}{b^2 v^3}. \quad (\text{A4})$$

By conservation of momentum, $\Delta p_{\parallel} = -\Delta P_{\parallel}$, so the large particle also experiences a backward deflection. The change in velocity for this large mass is $\Delta V = -\Delta p_{\parallel}/M$.

If the large mass were equally divided into n smaller masses such that the impact parameters were the same, equation A2 tells us that the deflection Θ would be:

$$\Theta = \sum \frac{2GM/n}{bv^2}, \quad (\text{A5})$$

where the sum is over the n particles. This deflection angle is equal to equation A2. Consequently, the momentum for any mass M is the same as it would be if the large mass were equally divided, despite the apparent M^2 dependence. Likewise, if the small mass m were divided into n equal masses, the momentum of mass m as a whole is determined by the sum of n deflections, and is equivalent to the unpartitioned momentum.

To get the force on the small mass, we can use Newton's 3rd law and find the

acceleration of the large mass, dV/dt . When the small mass is subdivided into n particles with number density η , this acceleration is:

$$\frac{dV}{dt} = - \int \frac{2G^2 M m}{b^2 v^3} 2\pi b db \eta v, \quad (\text{A6})$$

which simplifies to:

$$\frac{dV}{dt} = - \frac{4\pi G^2 M \rho}{v^2} \ln \Lambda \quad (\text{A7})$$

where $\ln \Lambda$ is the usual Coulomb logarithm. For a gaussian spectrum of velocities, equation A6 results in the dynamical friction acceleration, dv_f/dt , in equation 3 in the paper. Hence, the dynamical friction force on a secondary can be equally apportioned among equal mass secondary particles.

Fig. 1.— Final secondary density for a purely stellar 10:1 merger with and without secondary mass loss. The density of the secondary is shown as a function of radius after the merger. The density which results from neglecting secondary mass loss in the orbital decay trajectory is a dashed line, and the density which results from including this mass loss is a solid line. The changes are fluctuations due to small number statistics.

Fig. 2.— The xy plane projection of a secondary as it merges with a primary 10 times more massive on a $\kappa = 0.0$ encounter. Each panel represents a different snapshot of the bound secondary particles along its orbital decay trajectory. The last panel represents the distribution of unbound particles by the end of the merger. The separation of the primary and secondary is shown on the bottom of the plot. Most of the envelope particles are unbound after the first pass, and by the second pass, 90% of the matter is stripped away. However, the innermost particles remain bound to the secondary’s potential for several more passes, until the secondary is entirely disrupted, and the debris is distributed over a large volume of space.

Fig. 3.— The change in the secondary energy versus number of pericenter passes. We plot the change in the secondary energy (normalized by the initial secondary energy) versus the number of pericenter passes for the 10:1 $\kappa = 0.0$ merger. The square points are derived from our n-body simulation, and the solid line results from an impulse approximation expression for the change in secondary energy induced by the black hole. The secondary is clearly disrupted after 10 passes.

Fig. 4.— Density profile for the mass ratio 10:1 $\kappa = 0.0$ encounter. In the top panel, we illustrate the change in the inner density profile of the secondary. We plot the density at a radius r against radius in parsecs. The solid line is the final secondary profile, the thick dashed line is the initial state of the secondary, and the dotted line is the density profile of the primary for comparison. In the bottom panel, the thick solid line represents the resulting

remnant, the dotted line corresponds to the final state of the primary, and the thin solid line represents the final state of the secondary. The dramatically lower density in the secondary indicates it has been disrupted.

Fig. 5.— Density profile for the mass ratio 100:1 $\kappa = 0.0$ encounter. See caption for figure 4.

Fig. 6.— The xy plane projection of a secondary as it merges with a primary 100 times more massive on a $\kappa = 0.0$ encounter. See caption for figure 2.

Fig. 7.— Density profile for the mass ratio 100:1 $\kappa = 0.05$ experiment. See caption for figure 4.

Fig. 8.— Density profile for the mass ratio 10:1, $\kappa = 0.0$ experiment with negligible primary black hole mass. See caption for figure 4. Inside the tidal radius, the secondary is essentially intact.

Fig. 9.— The xy plane projection of orbital decay trajectories. The orbital decay trajectories for the secondary in the 100:1 $\kappa = 0.05$, 100:1 $\kappa = 0.5$, 10:1 $\kappa = 0.2$, and 10:1 $\kappa = 0.8$ experiments are shown in panels A, B, C, and D, respectively.

Fig. 10.— Density profile for the 10:1, $\kappa = 0.2$ experiment See caption for figure 4.

Fig. 11.— Density profile for the 10:1, $\kappa = 0.8$ experiment See caption for figure 4.

Fig. 12.— Density profile for the 100:1, $\kappa = 0.5$ encounter. See caption for figure 4.

Fig. 13.— Prediction of final secondary state for the $\kappa = 0.5$ orbit as a function of primary galaxy mass and central density slope. The dashed line marks the boundary between secondary destruction and survival.

Fig. 14.— The xy projection of the secondary galaxy viewed in the primary frame for the

10:1, $\kappa = 0.8$ experiment. See caption for figure 2. The leading direction of the secondary distortion indicates that the secondary is spinning, and that the spin may be induced by the black hole.

Fig. 15.— The xz plane projection of a secondary as it merges with a primary 10 times more massive on a $\kappa = 0.2$ orbit. See caption for figure 2. The secondary experiences significant flattening during the final pericenter pass (frame 4), and the particles are unbound to secondary once it has settled to the primary center (frame 5). The last frame illustrates that the debris remains tightly bound to the primary center.

Fig. 16.— The increase in secondary spin for the 10:1, $\kappa = 0.2$ experiment. We plot the azimuthal velocity of the secondary over the velocity dispersion versus time for a portion of the merger. The rapid increase of the circular velocity indicates that the secondary is spinning up over this time period.

Fig. 17.— The preferential loss of high angular momentum particles. We plot the energy versus the angular momentum of secondary particles in the secondary frame for different times in the 10:1, $\kappa = 0.2$ experiment. The angular momentum of the secondary sharply increases during the last orbit, and the particles with the highest angular momentum become unbound. In the last frame, the high angular momentum particles were stripped before the secondary reached the primary center. A few secondary crossing times after the secondary reached the primary center, the more plunging orbits were stripped, but still remained tightly bound to the primary.

Table 1. Eta Model Galaxy Parameters

$\frac{M_1}{M_2}$	Galaxy	M_V	$r_{\text{core}}^{\text{a}}$	$M_{\text{core}}^{\text{b}}$	η_{core}	r_{env}	M_{env}	η_{env}	r_{half}	M_{bh}
100:1	Primary	-22.0	263	4.7×10^{10}	2.15	4000	3.4×10^{12}	2.2	10617	6.3×10^9
				1.34			98.66			0.18
	Secondary	-18.0	3.8	1.6×10^8	1.0	300	3.5×10^{10}	1.5	508	
				4.4×10^{-3}			0.996			
10:1	Primary	-21.5	155	2.3×10^{10}	1.96	4000	1.9×10^{12}	2.0	9506	3.2×10^9
				0.117			9.88			0.02
	Secondary	-19.5	18.63	1.3×10^9	1.23	1029	1.95×10^{11}	1.5	1734	
				6.7×10^{-3}			0.993			

^aradii are in units of pc.

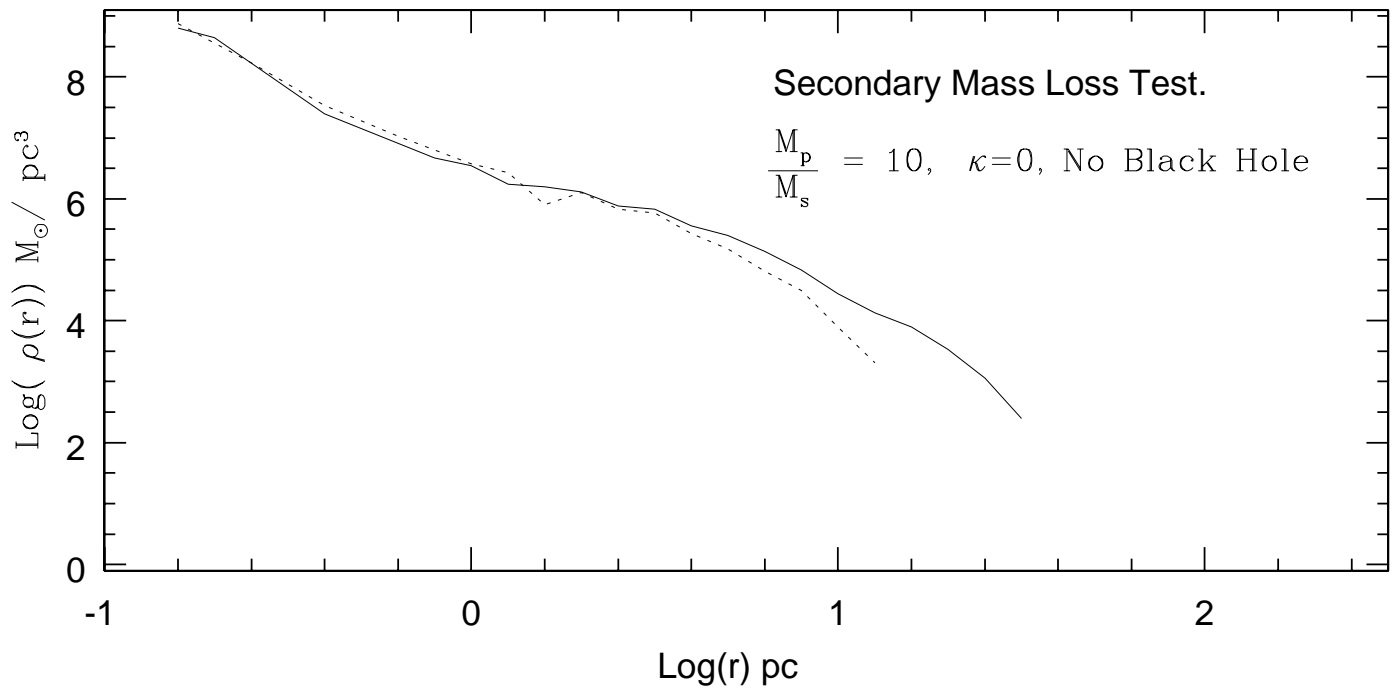
^bthe top masses are in units of M_{\odot} , and the bottom masses are normalized such that the total secondary mass is 1.0

Table 2. Secondary Spatial Resolution

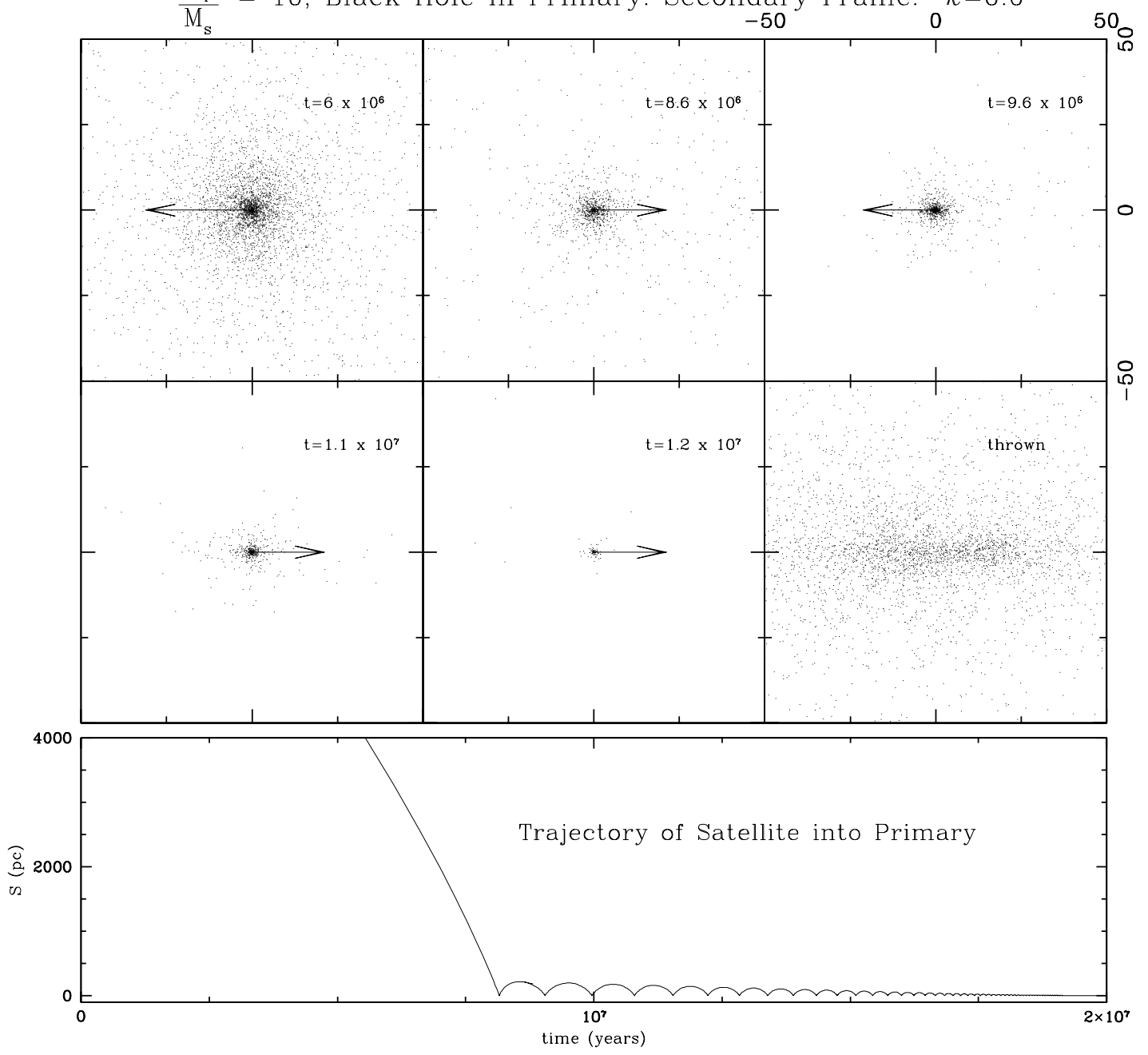
$M_1 : M_2$	Type	Particle Number	Resolution (pc)
100:1	Double η	5000	10.08
	Inner η	2000	0.07
		5000	0.05
10:1	Double η	5000	37.79
	Inner η	2000	0.57
	Inner η	5000	0.42
2.5:1	Double η	5000	119.6
	Inner η	2000	3.04
	Inner η	5000	2.24

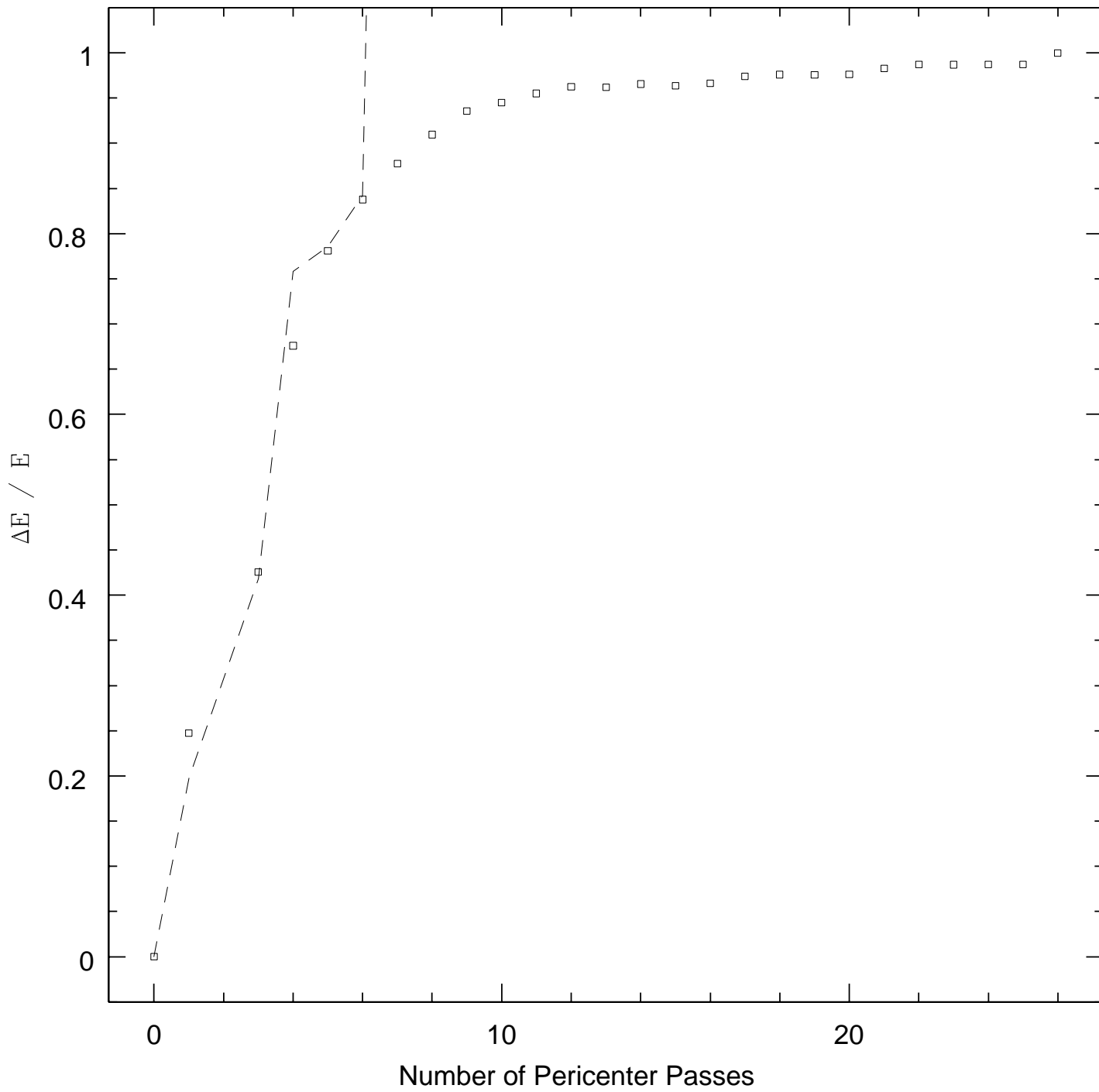
Table 3. Synopsis of Experiments

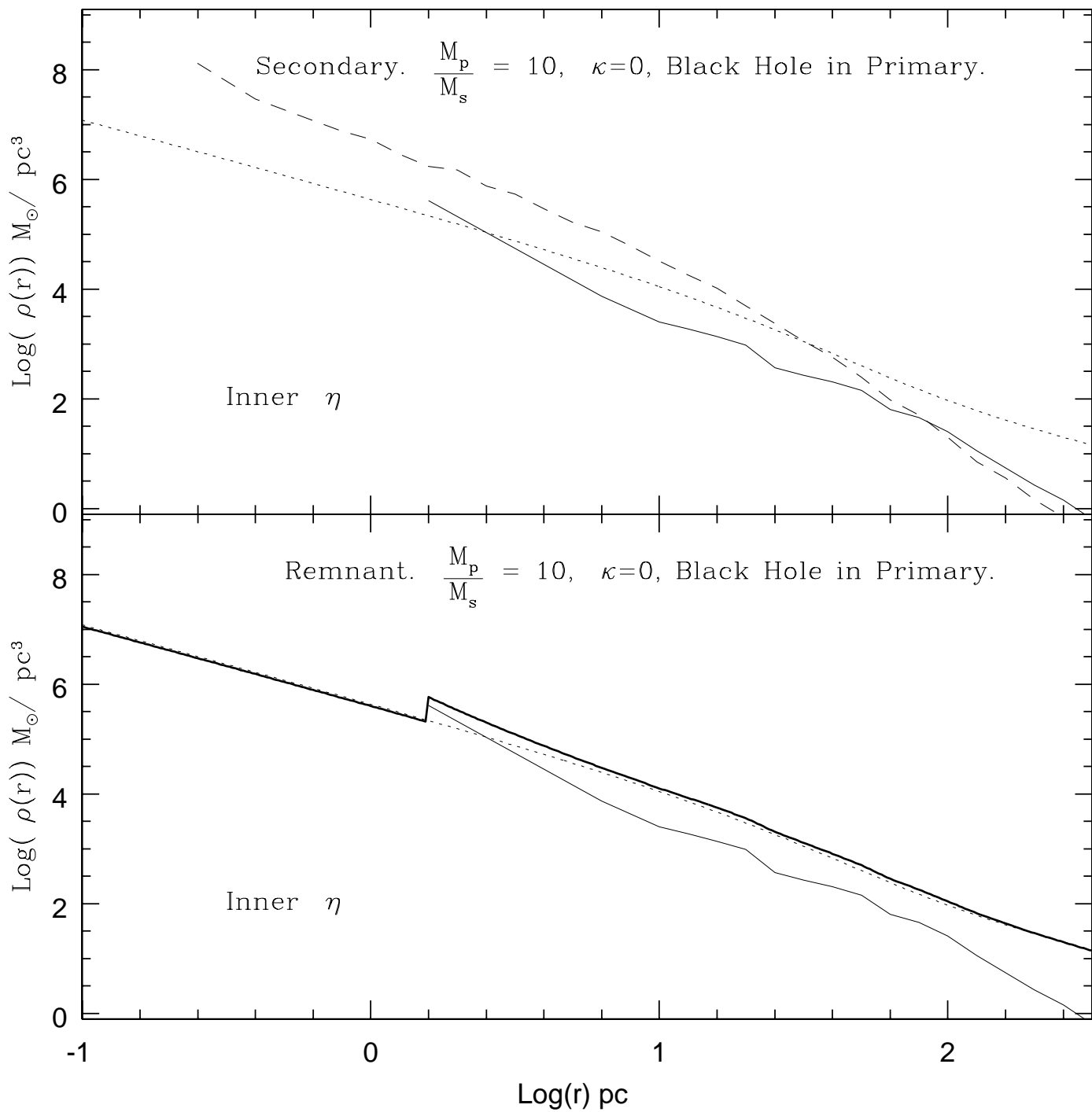
Mass Ratio	Initial apo:peri	κ	Black Hole Mass	Effect on Secondary
100:1	31850:0	0.0	0.18	Disrupted
	31850:460	0.05	0.18	Disrupted
10:1	28520:0	0.0	0.02	Disrupted
	28520:0	0.0	0.0005	Intact
100:1	31850:8650	0.5	0.18	Disrupted
10:1	28520:1640	0.2	0.02	Intact, spinning
	28520:14280	0.8	0.02	Intact, spinning

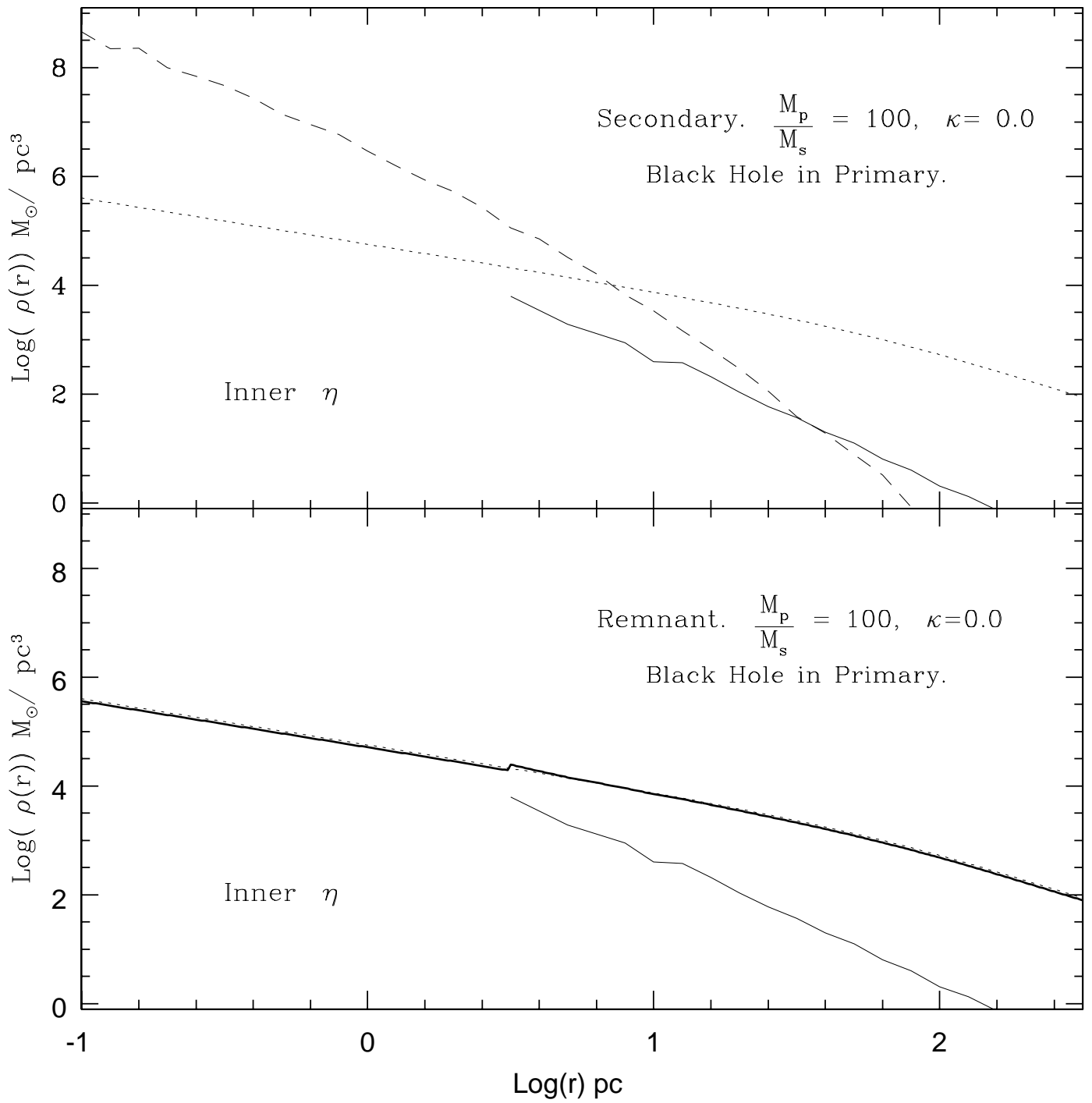


$\frac{M_P}{M_S} = 10$, Black Hole in Primary. Secondary Frame. $\kappa=0.0$

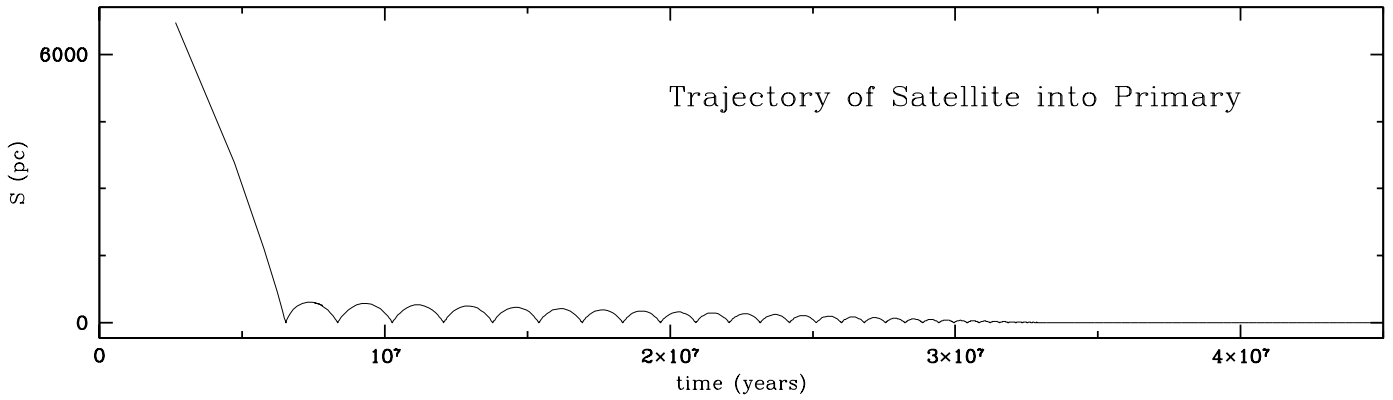
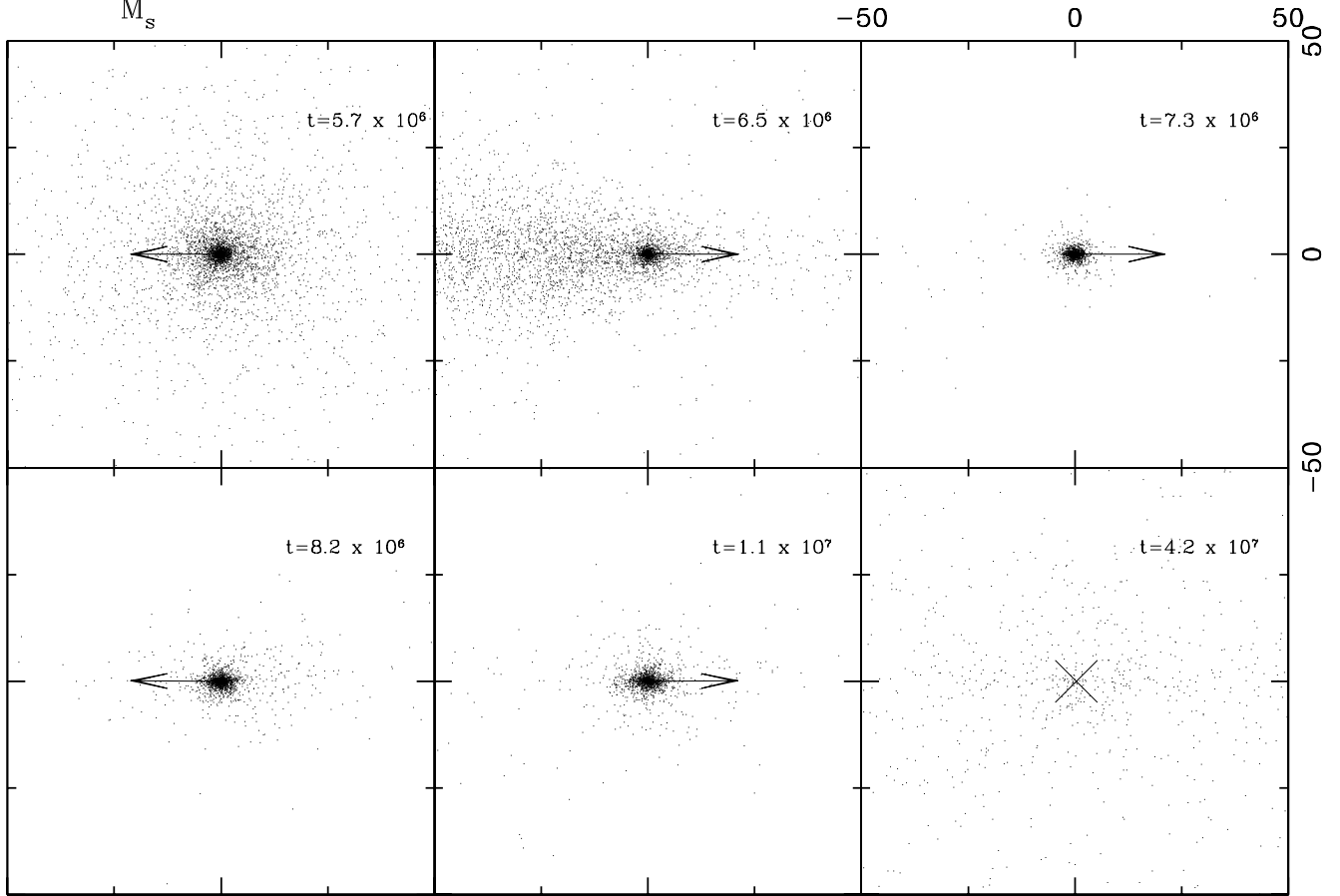


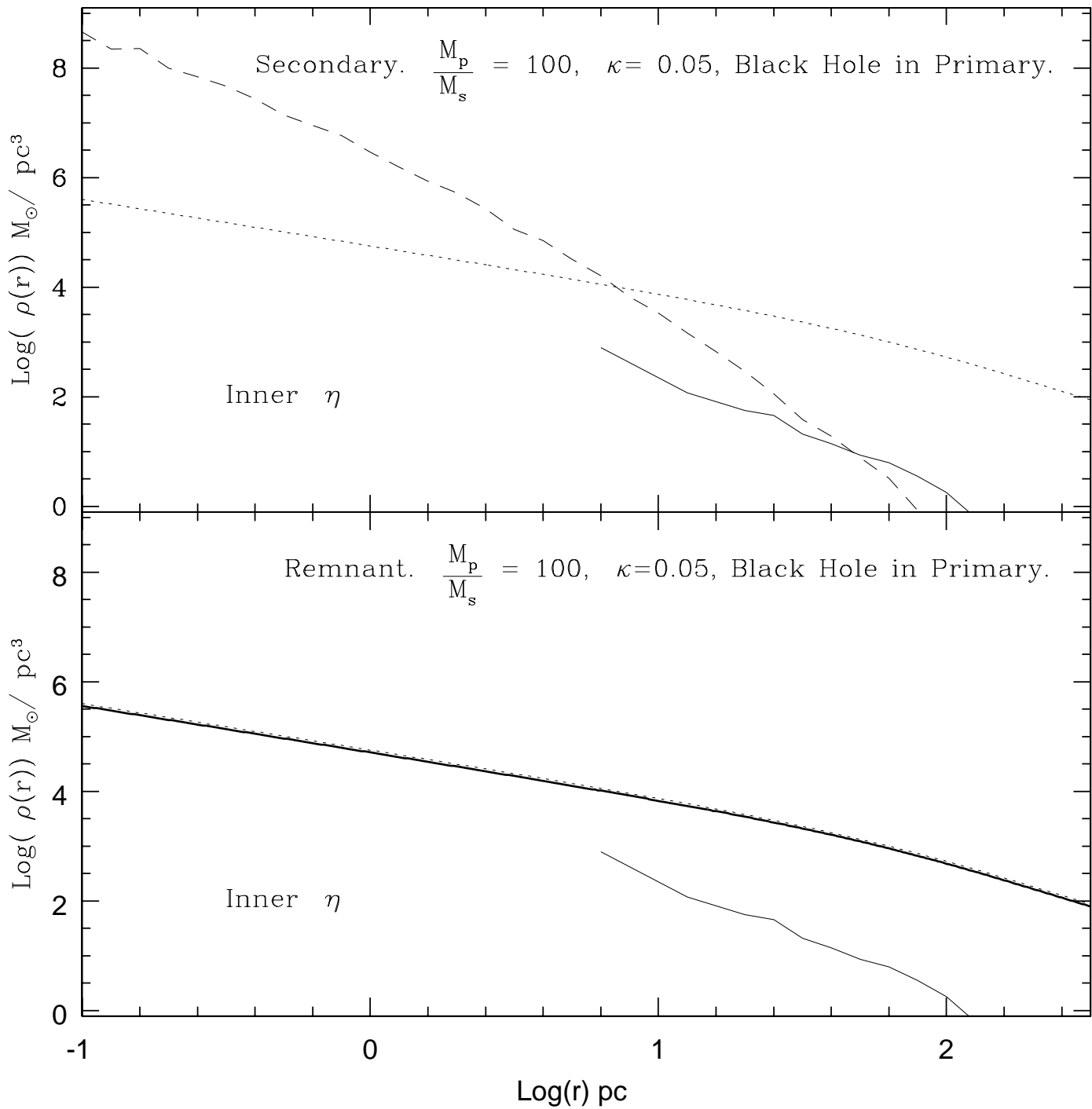


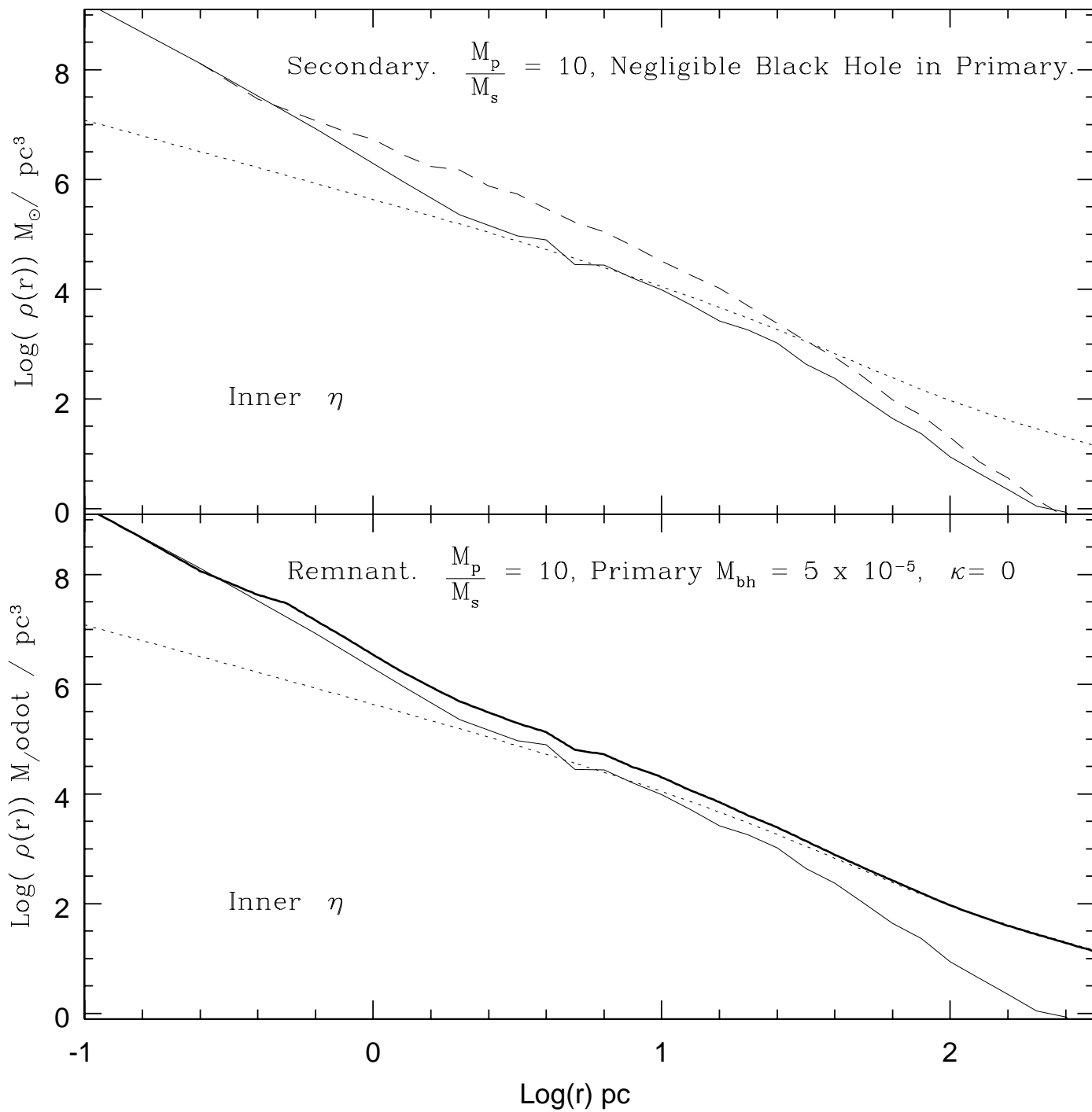




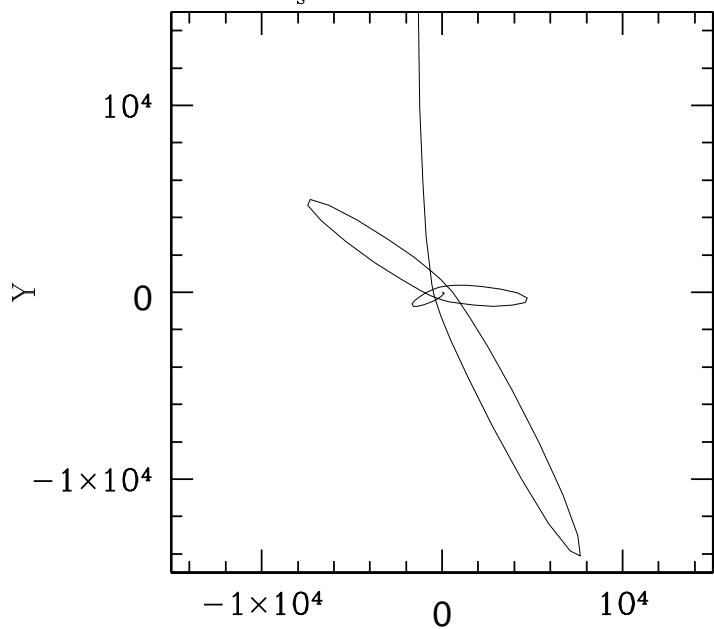
$\frac{M_P}{M_S} = 100.0$, Black Hole in Primary. Secondary Frame. $\kappa=0$.



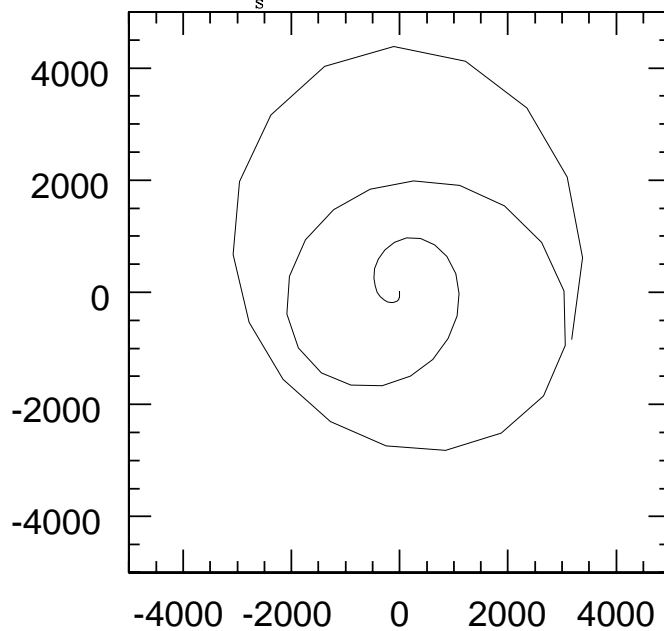




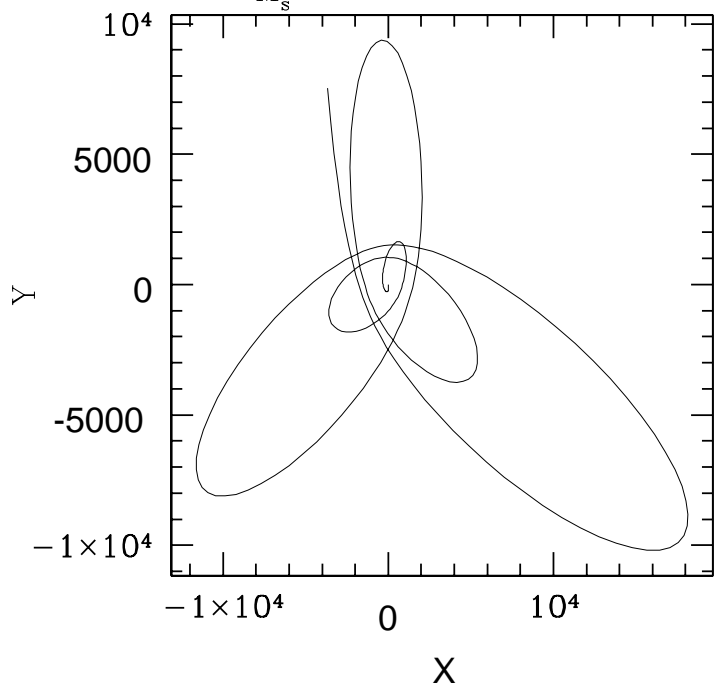
$$\frac{M_p}{M_s} = 100, \quad \kappa = 0.05$$



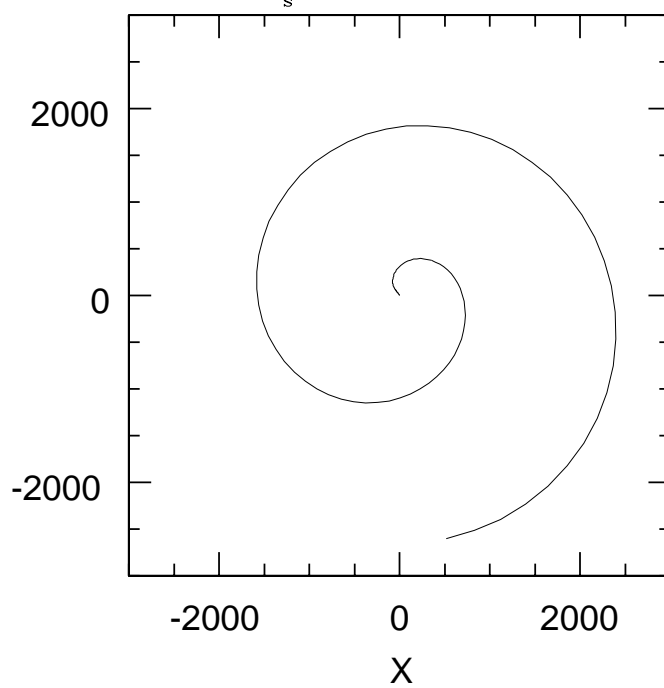
$$\frac{M_p}{M_s} = 100, \quad \kappa = 0.5$$

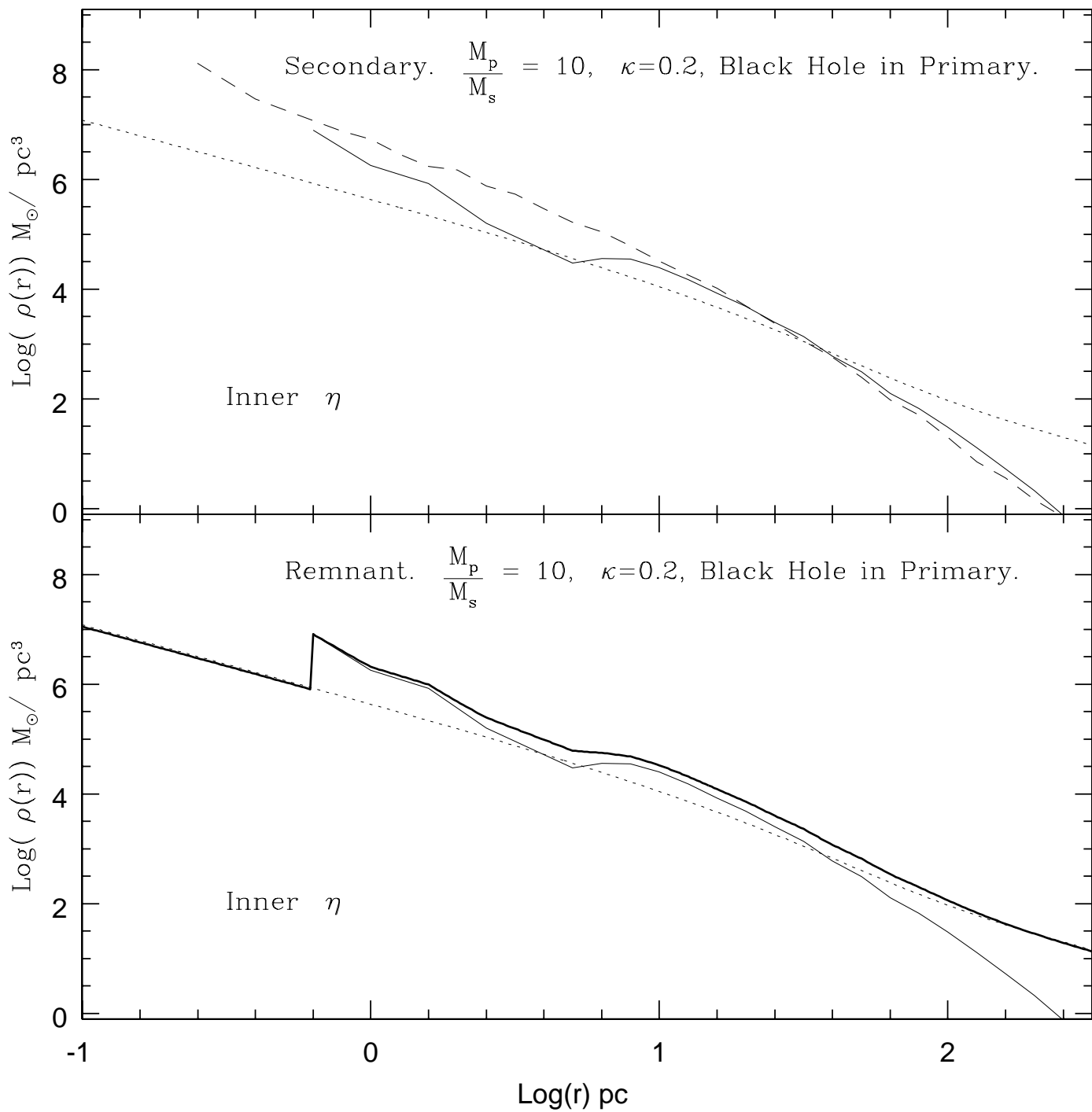


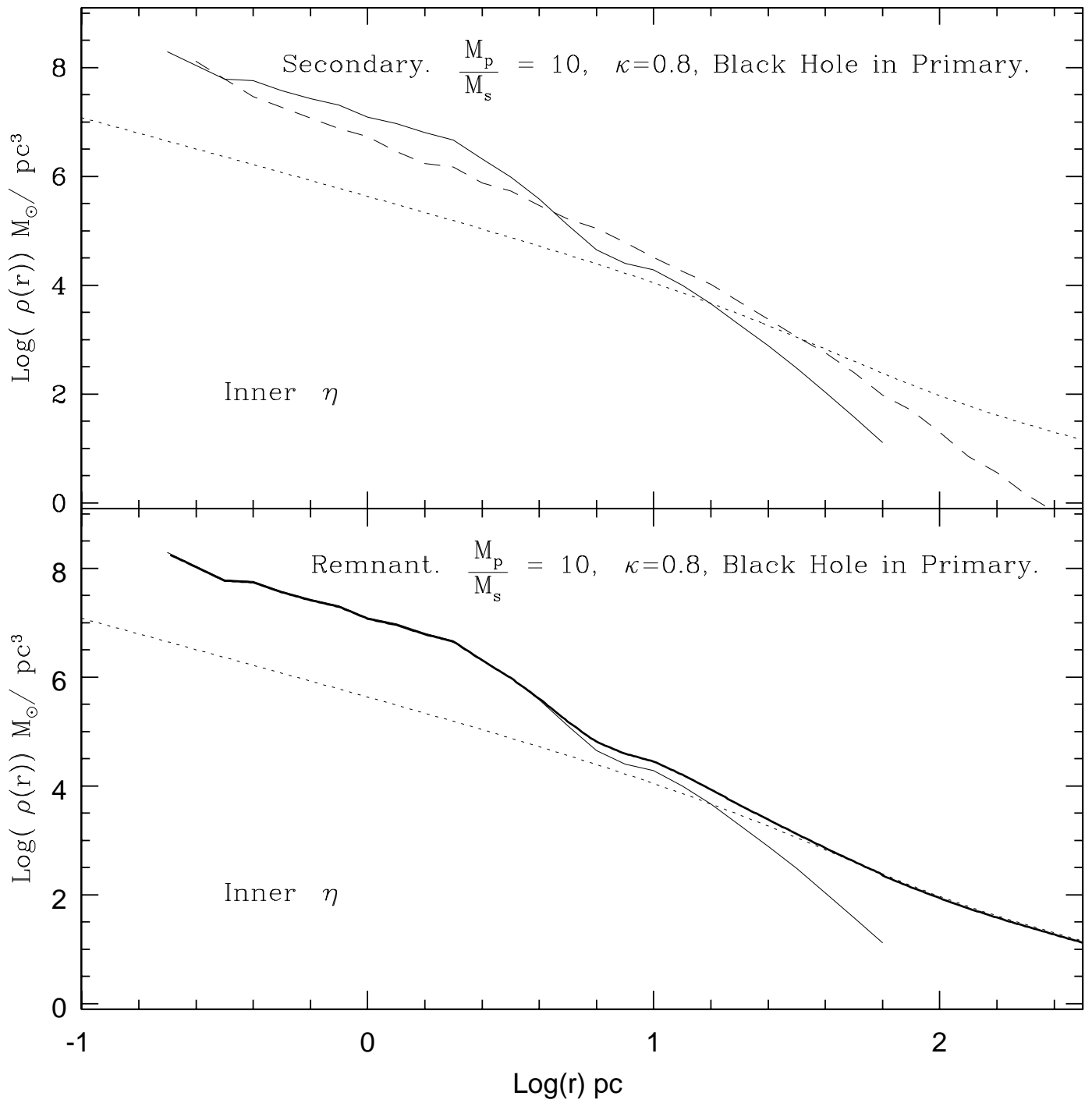
$$\frac{M_p}{M_s} = 10, \quad \kappa = 0.2$$

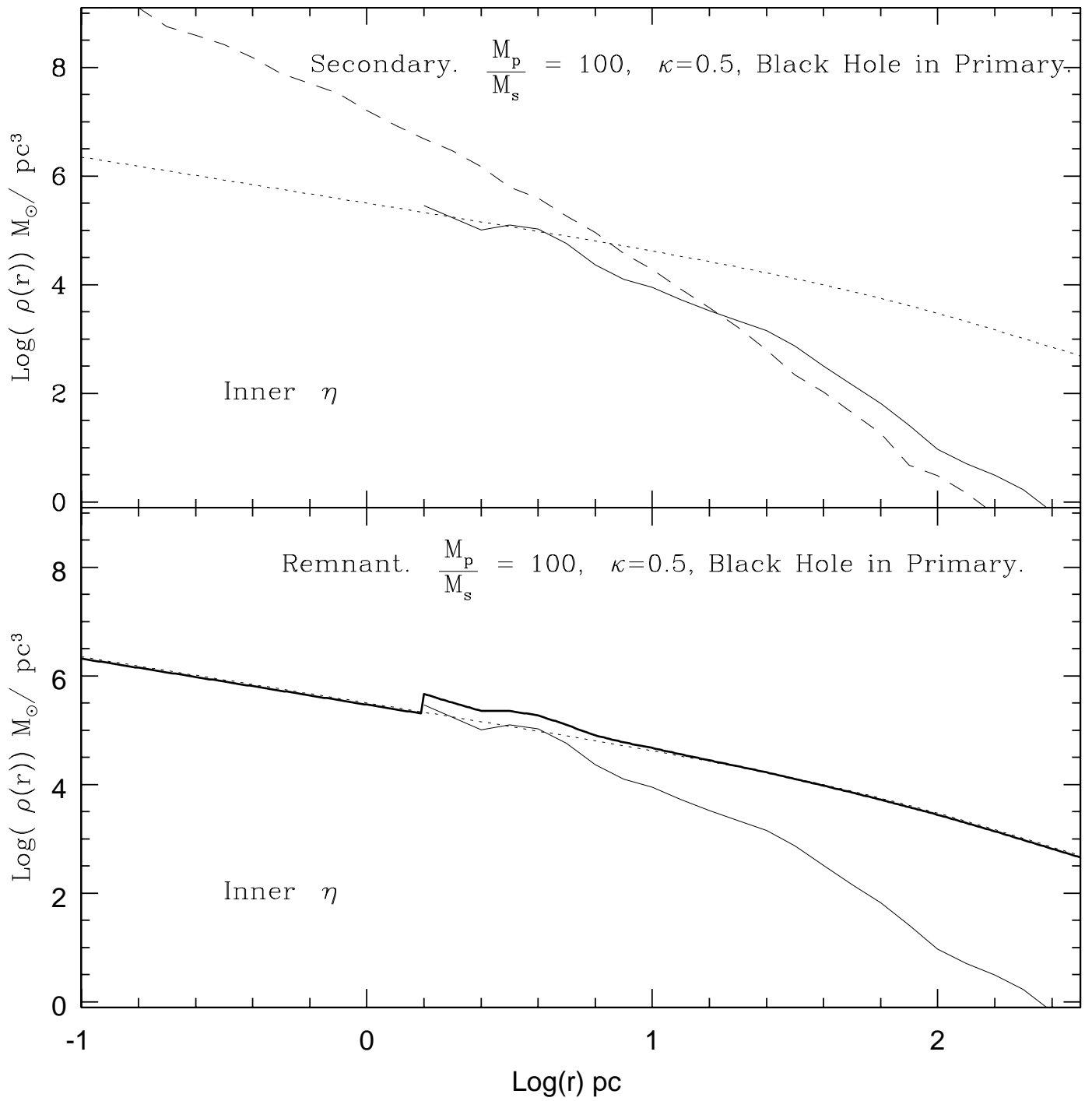


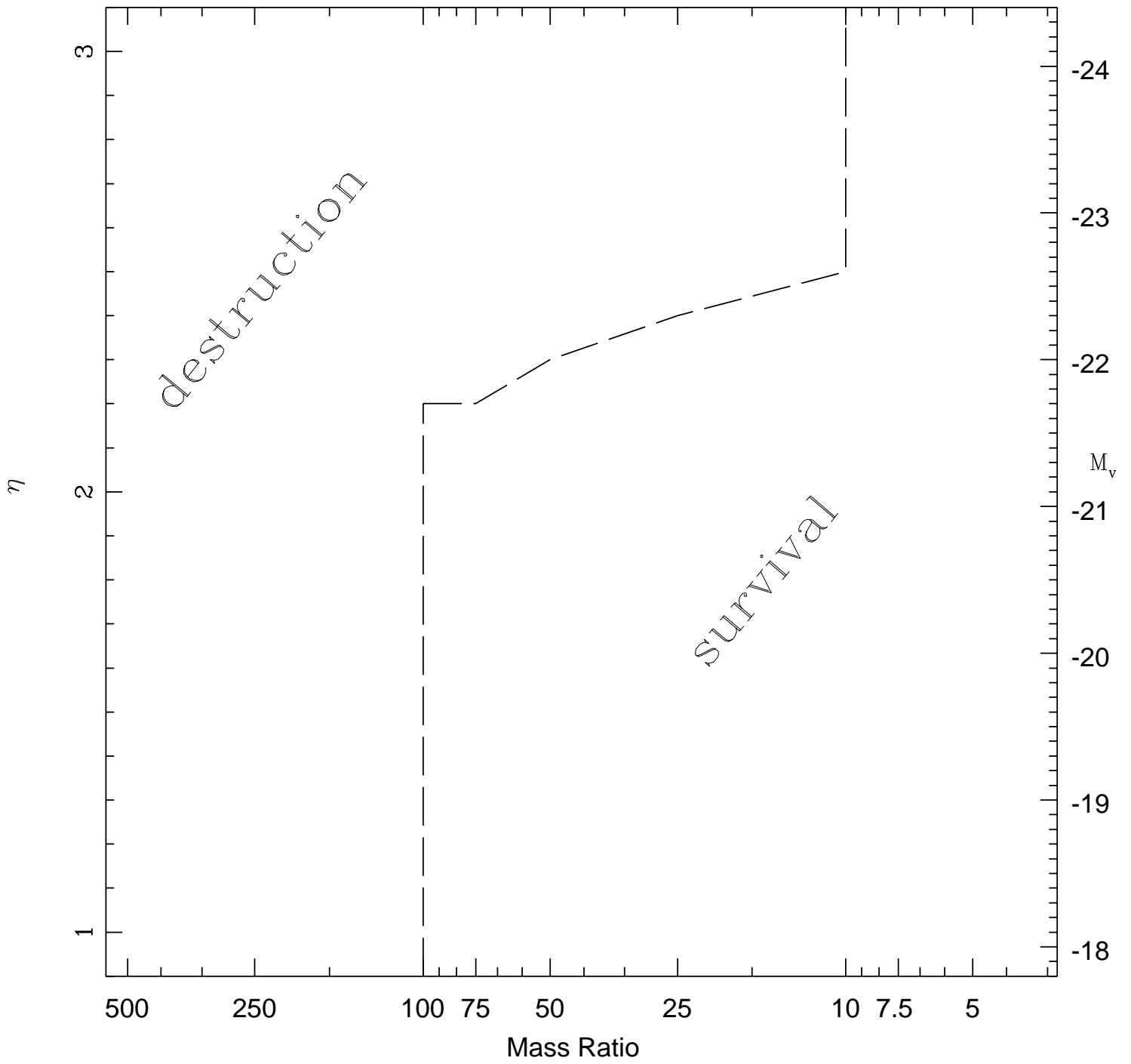
$$\frac{M_p}{M_s} = 10, \quad \kappa = 0.8$$



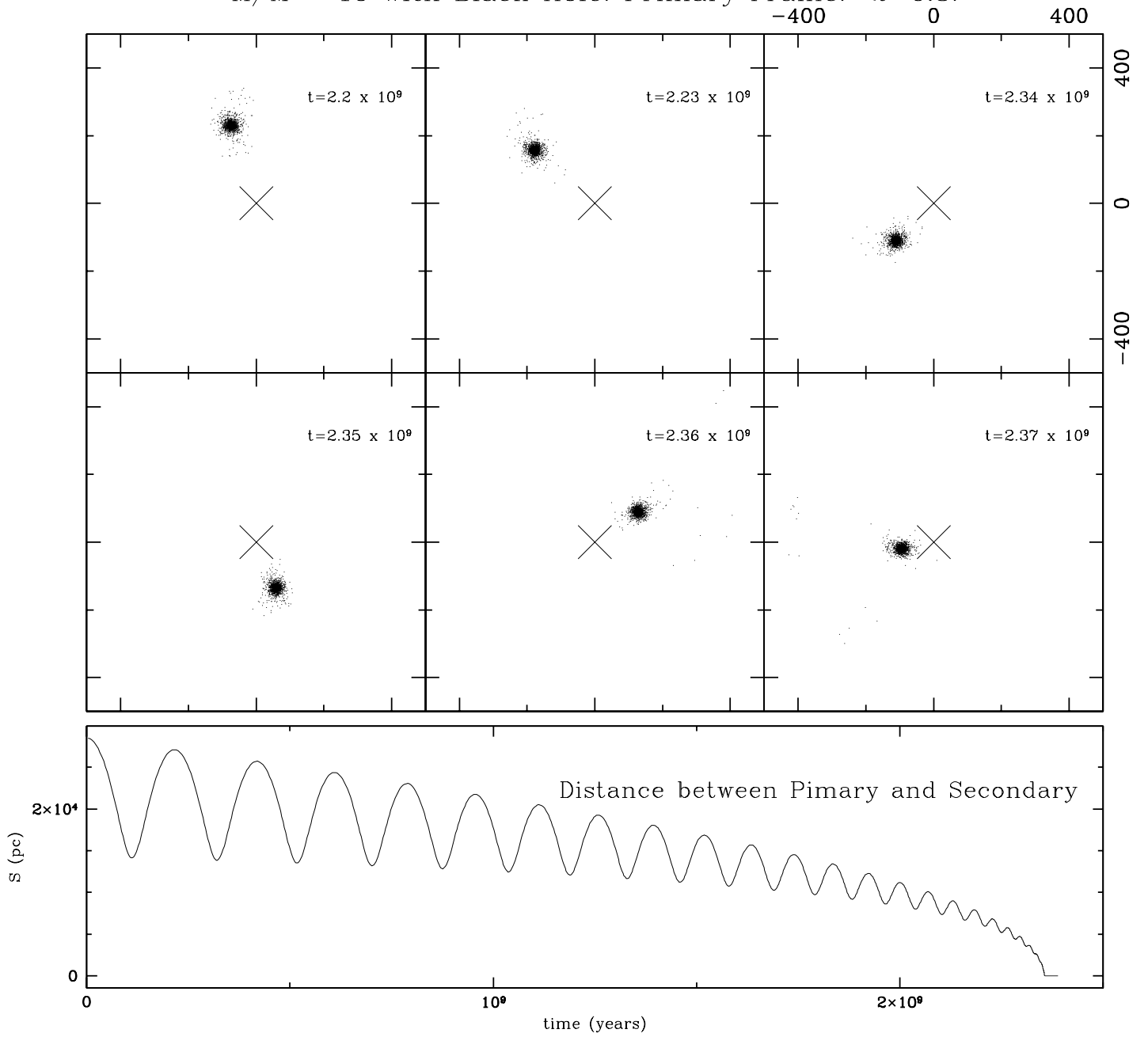








M/M = 10 with Black Hole. Primary Frame. $\kappa=0.8$.



M/M = 10 with Black Hole. Secondary Frame. $\kappa=0.2$.

